Journal of Coastal Research	13	4	983–994	Fort Lauderdale, Florida	Fall 1997

Salinity Intrusion In The Fly River Estuary, Papua New Guinea

Eric Wolanski, Brian King and Duncan Galloway

Australian Institute of Marine Science
P.M.B. No. 3
Townsville M.C.
Queensland 4810, Australia

ABSTRACT

WOLANSKI, E.; KING, B., and GALLOWAY, 1997. Salinity intrusion in the Fly River Estuary, Papua New Guinea. *Journal of Coastal Research*, 13(4), 983–994. Fort Lauderdale (Florida), ISSN 0749-0208.

Intensive field and model studies were undertaken into the dynamics of the Fly River estuary, Papua New Guinea. The estuary has three dominant channels forming a shallow, fan-shaped delta, and receives a mean freshwater discharge of approximately 6,000 m^3s^{-1} with little seasonal variation. The estuary is vertically well-mixed in salinity by strong tidal currents. The saline water is distributed unevenly between the channels. Model studies verified by field data suggest that this due to the dynamics of the estuary which are controlled by shallow water frictional effects that generate higher tidal harmonics, the shoaling of the tidal wave from the funnel shape of the estuary, a low value of the bottom friction coefficient resulting from the presence of fluid mud, and the along-channel water surface gradient. This gradient is in turn controlled by two dominant forcings, namely the freshwater discharge and the dominant offshore trade wind. This gradient is also modulated by the spring-neap cycle of the tidal currents which controls the low-frequency friction coefficient. The absence of strong cross-channel salinity gradients and of axial convergence zones is attributed to enhanced horizontal mixing by the lateral velocity shear due to the sinuosity of the thalweg meandering between numerous islands and shoals.

ADDITIONAL INDEX WORDS: *Estuary, salinity, tides, asymmetry, friction, wind stress, model, Papua New Guinea.*

INTRODUCTION

The Fly River estuary in Papua New Guinea (Figure 1) has a fan-shaped delta with three distinct channels and numerous islands. The channels are the Far Northern, Northern and Southern Channels. The estuary is shallow throughout with depths < 10 m in the thalweg and more commonly < 5 m. The freshwater discharge is about 6,000 m^3s^{-1} with small (typically $\pm$ 1,500 m^3s^{-1}) seasonal variations. The mean suspended sediment concentration in the freshwater region is typically 0.5–1.0 g l^{-1} (SALOMONS and EAGLE, 1990; OTML, 1988; WOLANSKI *et al.*, 1995). The tidal limit extends no more than 150 km upstream of Lewada located at the apex of the delta (Figure 1). Previous information on the estuarine dynamics of the Fly River was minimal, being limited to a dozen CTD observations by TAYLOR (1973), tidal observations at three points for a few months as part of a navigation study (SMEC, 1982), and more recently, occasional CTD observations in the Far Northern Channel only (OTML, 1988).

From December 1989 to mid-1992 we undertook a detailed study of the dynamics of the Fly River estuary as part of a water quality investigation (WOLANSKI and EAGLE, 1991). Observations on the dynamics of the tidal and non-tidal circulation and the salinity regime are presented here. These data are used to verify a mathematical model of the hydrodynamics and the salinity distribution in, the Fly River estuary. The hydrodynamic processes explain the uneven distribution of the salinity in the three channels, and in turn the uneven salinity distribution controls the variable distribution of mangroves along the three channels.

95069 received 30 May 1995; accepted in revision 5 November 1995.

METHODS

Eight cruises have been undertaken, each of typically 10 days to two weeks duration. During 1990 and 1991, exploratory cruises were conducted over the entire estuary at 3–4 month intervals. During 1992, three cruises were completed within a 11 week period which were focused on the Southern Channel. A bathymetric chart was obtained from SMEC charts for the Far Northern Channel. For the other two channels we surveyed about twenty cross-sections and a number ($\approx$ 50) of single point measurements of depth.

Bottom-mounted Aanderaa water levels recorders were deployed throughout the estuary (Figure 1) and were maintained for periods of up to two years. Bottom-mounted frames, 2m high, containing one or two vector-averaging current meters (model Inter-Ocean S4 and Steedman CM01), were deployed in the estuary at sites alpha, beta, gamma and delta (Figure 1) for periods of up to 11 weeks, and for shorter periods (1–2 weeks) at stations P, Q and S. Backscatter nephelometers were deployed in conjunction with the frame-mounted current meters to measure the suspended sediment concentration at 2 or 3 elevations above the bottom (WOLANSKI *et al.*, 1995; WOLANSKI and GIBBS, 1995). Some moorings were damaged by river debris, including entire tree logs that are commonly seen floating in the estuary. An Aanderaa

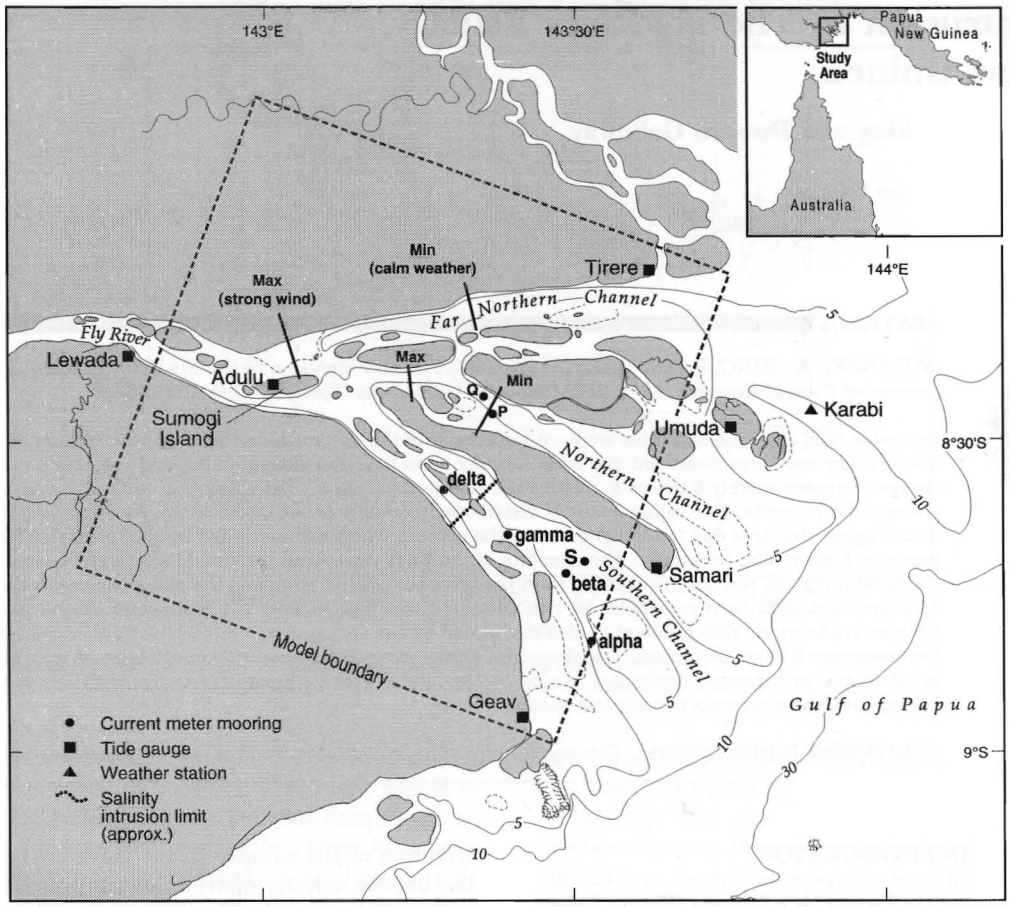

Figure 1. Location map of the Fly River estuary, depths contours (heavily smoothed, in m), some measurement sites, and model boundary (dotted lines). The Max and Min lines in the Far Northern and Northern Channels are the locations of the observed maximum and minimum salinity intrusion limits. The line near site delta in the southern channel represents the location of the mean salinity intrusion limit.

weather station was installed and calibrated on the concentrate vessel "Karabi", moored at the mouth of the Far Northern Channel (Figure 1).

Profiles of salinity, temperature, and suspended sediment concentration were collected at 12 stations over one or two tidal cycles, at hourly or half-hourly intervals This was undertaken using a CTD-cum-nephelometer profiler (WOLANSKI *et al.*, 1988) for very turbid estuarine waters and, when the waters were less turbid, using a Seabird CTD profiler which was also fitted with an optical backscatter nephelometer. By this technique, we measured the along-channel, and occasionally the cross-channel, distribution of salinity, temperature and suspended sediment in each of the channels. At a few anchor stations, a current meter was suspended 3 m below the ship, recording velocity at 10 minute intervals. At two anchor stations, an InterOcean S4 current meter logging data continuously was lowered through the water column in order to obtain vertical profiles of the current distribution at half-hourly intervals over one or two tidal cycles. Sail drogues 1 m × 2 m were deployed in the estuary and radar-tracked to measure the water circulation at the apex of the delta.

Tidal harmonic analysis (FOREMAN, 1977) was used to calculate tidal constants for water level and current data. These constants were then used to calculate time series of tidally-predicted water levels and currents. Time series of residuals were obtained by subtracting the tidally predicted time series from the observed ones. Time series of low-frequency water level and currents were obtained by applying the GODIN (1972) moving average filter, $A_{24}{}^2A_{25}/24^225$, to the time series. The coherence computations follow the procedure of RAUPACH and MITCHELL (1977).

Wind velocity components are positive if eastward (x-axis) or northward (y-axis). The convention used for current data collected within the river defines the x-axis to be in the general along-river axis with flood tidal currents being positive.

FIELD RESULTS

Wind

The dominant wind was the trade wind which blows from the sea parallel with the axis of the Far Northern Channel. Generally, the wind blew from the northwest during the sum-

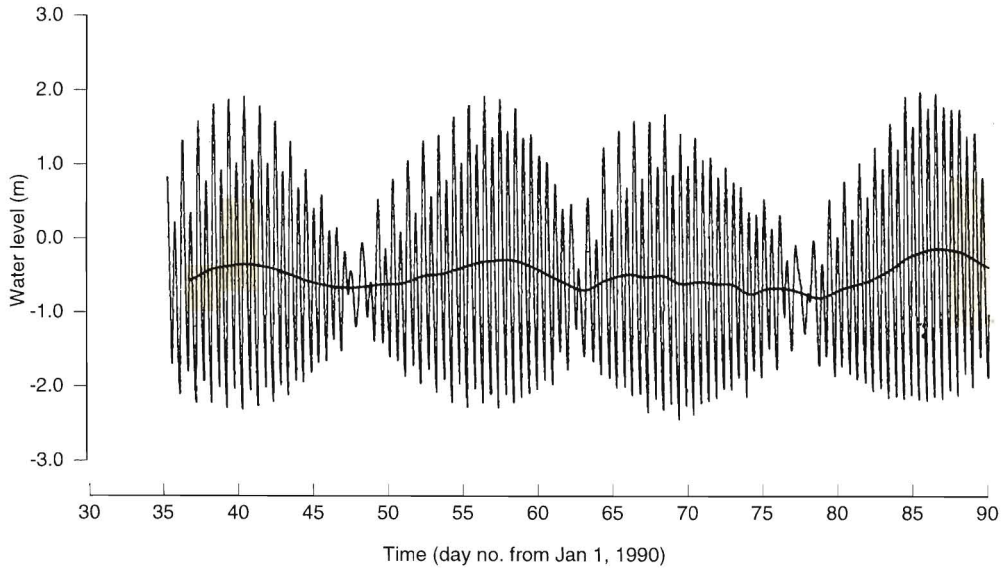

Figure 2. Time series plot of the water level (thin line = raw data; thick line = low-frequency) at Adulu near the apex of the delta.

mer monsoon and from the southeast throughout the (dominant) winter trade wind season. The wind velocity spectra (not shown) reveal that the wind was energetic at periods of days to weeks; periods of calm weather were short (< a few days typically) and rare (WOLANSKI *et al.*, 1994).

Planetary Tides

The tides are semi-diurnal, with a large diurnal inequality and a strong spring-neap variation (Figure 2). Peak to trough fluctuations were up to 4 m during spring tides and about 1 m at neap tides. Tidal harmonic calculations (Table 1) show that the M_2 tide was by far dominant, followed by the S_2 tide and, of nearly equal magnitude, the N_2 and K_1 tide. The latter two constituents were present with a similar amplitude at the mouth. The tides were practically the same at the mouth of each of the three channels (not shown). The amplitude of the dominant diurnal and semi-diurnal tidal components (*e.g.*, M_2, S_2, K_1 and O_1) was about the same at the mouth and at the apex of the delta (Table 1), but the N_2 tide varied somewhat more along the channel.

Table 1. *The amplitude (A, in m) and phase (ϑ, in °) of the major constituents from tidal measurements within the estuary at the river mouth (Tirere) and at the apex of the delta (Lewada).*

	River Mouth (Tirere)		Apex of the Delta (Lewada)	
	A	ϑ	A	ϑ
M_2	1.049	341.7	1.080	64.4
S_2	0.587	321.3	0.598	42.7
N_2	0.327	323.8	0.266	43.8
K_1	0.312	211.2	0.313	262.6
O_1	0.161	159.7	0.187	197.7
M_{sf}	0.052	8.0	0.182	356.6
M_4	0.02		0.16	
S_4	0.01		0.17	
MN_4	0.012		0.16	
M_8	0.001		0.32	

Higher harmonics tides were small at the mouth but became important at the apex of the delta where the $M_4 + S_4$ tides reach 0.33 m. This amplitude is 10 times that at the mouth of the estuary. Even higher harmonics became important, for instance the M_8 tide amplitude was 0.32 m at the apex of the delta as opposed to 0.001 m at the mouth (Table 1). Presumably these higher harmonics were generated by friction in shallow waters (AUBREY and FRIEDRICHS, 1988).

During neap tides, the tide at the apex of the delta lagged that at the mouth, but the tide was still essentially a semi-diurnal sinusoidal curve where the shallow water tidal components were not important. During spring tides, the tide at the apex of the delta was distinctly non-sinusoidal. At that point the flood tide duration was measurably shorter than the ebb tide duration, resulting in stronger flood than ebb tidal currents (Figure 3). The tidal asymmetry thus only became important at spring tides, presumably as a result of non-linear friction effects in shallow waters. The tides decreased in amplitude in each of the channels before meeting at the apex of the delta near Lewada where they grow again as a result of a funnelling effect. The shoaling and the funnelling effects combine to produce a tidal bore at the upper reaches of the estuary upstream from Lewada during the equinox spring tides

Low-Frequency Water Level

While diurnal and semi-diurnal tides were most obvious, there were also low-frequency fluctuations of water level reaching 0.2 m peak-to-trough at periods of days to weeks (Figure 2). At the mouth the low-frequency water level fluctuated at periods of typically 10 to 20 days with peak to trough amplitude typically 0.1 m. Oscillations were forced by

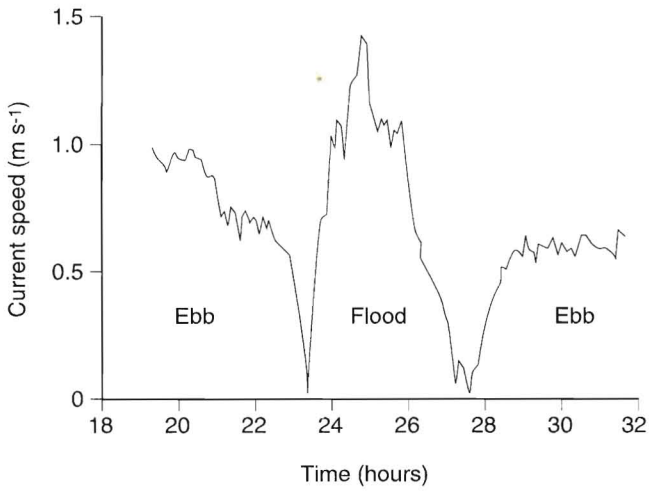

Figure 3. Time-series plot of the current speed in the thalweg at Adulu, Sumogi Island, in the freshwater region of the estuary, 14–15 December 1989.

the Gulf of Papua and the Coral Sea (WOLANSKI *et al.*, 1994). Oceanic low-frequency fluctuations of water level were also experienced at the apex of the delta in addition to other non-oceanic fluctuations. These additional fluctuations were readily measurable since they reached up to 0.2 m (Figure 4a) and indicated a fluctuating along-channel slope of the water surface. This difference was least (0.03 m) in calm weather and at neap tides.

The resulting difference in low-frequency water level between the mouth and the apex of the delta varied by as much as 0.2 m although the freshwater discharge remained about constant. When determining the cause of these fluctuations, it was apparent (Figure 2) that the low-frequency fluctuations at the apex of the delta were phase-locked with the spring-neap tide cycle; the low-frequency water level at the apex of the delta was generally higher at spring tides than at neap tides (Figure 2). This spring-neap tidal period was reflected in the M_{sf} tide being three times larger at the apex of the delta than at the mouth (Table 1). The apparent M_{sf} tide (spring-neap tide cycle) was not due to the freshwater discharge since the latter varied little and then only at monthly periods and not at two weeks period (not shown). Instead it can be attributed to the variation of the low-frequency bottom friction coefficient with the spring-neap tide cycle in shallow waters (PROVIS and LENNON, 1983; WOLANSKI, 1994). As a result, the along-channel mean water slope necessary to maintain the freshwater discharge was larger at spring tides than at neap tides (*i.e.*, varying at the M_{sf} frequency).

Another important parameter determining the mean water slope was the trade wind. The wind fluctuated at periods of typically 1–2 weeks, peaked at 15 m s^{-1} (30 knots) but more commonly 12 m s^{-1} (25 knots), and applied a fluctuating landward wind stress principally in the Northern and Far Northern Channels which are oriented nearly parallel to the trade wind direction.

Linear regression analysis suggested that the tidal range

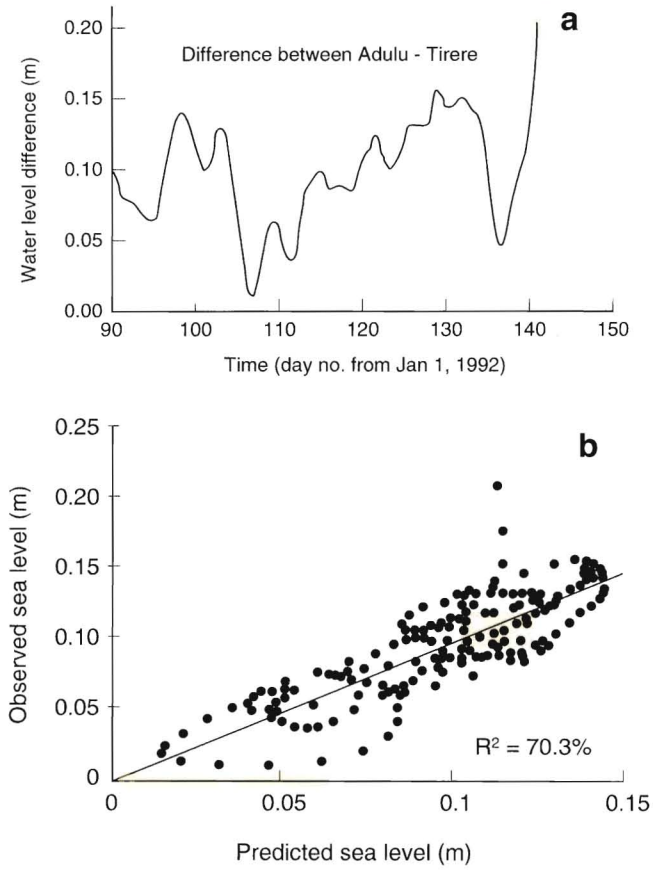

Figure 4. (a) Time series plot of the difference between low-frequency water level at the apex of the delta (Adulu) and at the mouth (Tirere). (b) Comparison between the observed and predicted low-frequency water level time series at the apex of the delta (Adulu).

alone does not explain satisfactorily the difference in the low-frequency water level between the mouth and the apex (R^2 = 0.3), nor did the wind alone ($R^2 < 0.3$). However, this water level difference is linearly dependent (R^2 = 0.73; Figure 4b) on both the maximum tidal range on that day and on the along-channel component of the wind velocity.

Currents

Vertical profiles of velocities near the mouth (Figure 5) showed little vertical shear except near the bottom as a result of friction. Buoyancy was not important in controlling the shear because the vertical salinity gradients were negligible. There was also a 1 to 2 hr lag between slack tide (labelled A) and slack tidal currents (balled B; see Figure 5). This lag became larger (up to 3 hours, not shown) near the apex of the delta.

Also apparent in Figure 5 is a small asymmetry between peak flood and ebb tidal currents. The tidal asymmetry was largest in the freshwater region (Figure 3) with measurably larger flood than ebb tidal currents. The largest peak tidal currents ($\approx$ 2 m s^{-1}) occurred during spring tides near the apex of the delta (not shown).

Salinity

The saline water was distributed unevenly between the three channels. Salt water propagated the farthest up-river in the Far Northern Channel, and the least in the Southern Channel, the salinity intrusion distance in the Northern Channel was intermediate between those in the Southern and Far Northern Channels (see the lines labelled Max and Min in Figure 1). The fluctuations of the saline intrusion distance were largest also in the Far Northern Channel, and least in the Southern Channel.

This asymmetry between the channels has important biological implications because it accounts for freshwater mangroves prevailing along most of the Southern Channel and saltwater mangroves along most of the Far Northern Channel.

The largest variability in stratification occurred in the Southern Channel. This channel was stratified during neap tides under light winds, it was vertically-well-mixed during spring tide and under trade winds (Figure 6). By contrast, the Far Northern Channel was vertically well-mixed during all our surveys (Figure 7) and in addition it showed large, apparently wind-driven, fluctuations in the salinity intrusion limit (Figure 1). The Northern Channel was generally vertically well-mixed. Cross-channel salinity changes seldom exceeded 0.5 ppt. Convergence zones as described by TURRELL and SIMPSON (1988) were only observed along shear lines generated by flow separation at islands.

A MODEL OF THE ESTUARINE CIRCULATION

The barotropic tidal currents are much stronger than the baroclinic currents. This suggests that the estuary can be modelled by adding the tidal, barotropic, depth-averaged, currents and the low-frequency, tidally- and laterally-averaged, baroclinic currents.

The Barotropic Hydrodynamic Model

We used the fully non-linear, depth-averaged, alternating direction implicit (ADI), finite difference, mass-conserving model of WOLANSKI and KING (1990) which is an adaptation of Leendertsee's classical model. The mesh size was 1410 m, the model boundary is shown in Figure 1, and the time step was 120 sec. The open boundaries were forced by observed, water level variations including the higher harmonics (Table 1).

Commonly used values of the Manning roughness coefficient, n (n = 0.025, a common value for sandy estuaries) generated an unrealistic standing wave. Small values of n (n = 0.015) produced a propagating tidal wave in close agreement with observations. With this small value of n, the model predictions were successfully verified both against water level time series data ($R^2 > 0.95$) and against current data from moored current meters ($R^2 = 0.87 - 0.93$; see Figure 8).

The small value of Manning's n in the Fly River may be due to the presence of fluid mud in the estuary (WOLANSKI *et al.*, 1995) enabling the bulk of the flowing water column to slip over the fluid mud layer, thereby decreasing bottom friction stresses.

The model suggests that the bathymetry is the key factor in tidal dynamics. The bathymetry generates the funnelling effect leading to an amplification of the tidal wave at the apex of the delta. The bathymetry (*i.e.*, the small depths) generates the higher tidal harmonics (*e.g.*, the. M_4 tide, see Table 1) on the tidal wave, giving rise to a tidal asymmetry which is most apparent near the apex of the delta. The model predicts that at ebb tide at least 80% of the discharge is diverted south of Sumogi Island. This prediction agrees with the observations of drogue tracks (Figure 9).

Internal Estuarine Flow

The laterally-averaged circulation was calculated using the model of FISHER *et al.*, (1972). This model fine tunes the eddy dispersion coefficients until a good agreement is found between observed and predicted salinity profiles. The predicted net water circulation is then derived. The predicted baroclinic currents are maximum at the river mouth and vanish at the salinity intrusion limit. This model neglects across-channel baroclinic currents (TURRELLL and SIMPSON, 1988); however such currents may not be of primary importance in the dynamics of the Fly River estuary because these currents would lead to along-channel fronts and these were seldom observed except near separation points at islands. As discussed below, mixing by lateral shear is intense and prevents the formation of cross-channel salinity differences > 0.5 ppt.

SALINITY MODELING

The hydrodynamics model was linked to a mass-conserving, particle-tracking, advection-dispersion model, to predict the fate of freshwater in the estuary. A particle tracking model was used instead of an Eulerian model because of the complex topography (MOELLER and ADAMS, 1993). The model tracks the positions of freshwater particles advected by the barotropic and baroclinic currents, assuming the freshwater particles are mainly located near the surface. Horizontal diffusion is parameterised by a random walk.

The model predictions are in close agreement with observations. Longitudinal salinity profiles, both observed and predicted, are shown in Figure 10 for the Southern Channel for which the data are the most extensive. For the Far Northern Channel, a close agreement is also found between the observed (Figure 1) and predicted (Figure 11) salinity intrusion limits in, respectively, calm weather and under strong winds. The predictions for the uneven distribution of salinity among the three channels (Figure 11) agree also closely the observed one (Figure 1), saline water penetrating the farthest in the Far Northern Channel especially under strong trade winds, and the least in the Southern Channel where wind-driven salinity fluctuations are the smallest.

By tracking freshwater particles in the model, the division of the freshwater discharge between the channels can also be evaluated. This division of the freshwater discharge is found to be significantly uneven. Indeed, the model predicts (not shown) that in calm weather the freshwater discharge is split about 55% in the Southern Channel, 35% in the Northern Channel and 10% in the Far Northern Channel. This split becomes 80% (Southern Channel), 15% (Northern Channel)

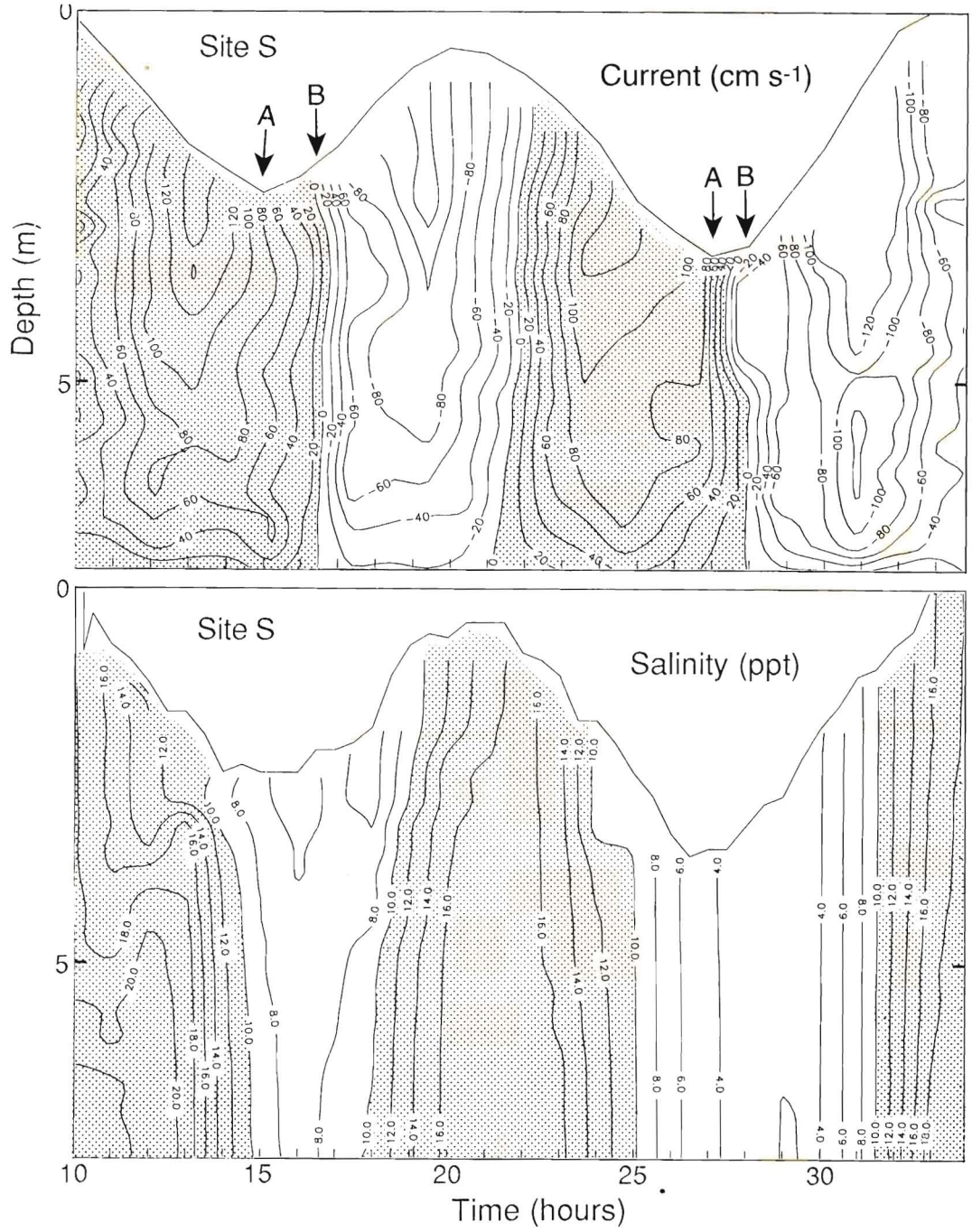

Figure 5. Time-series plot at site S showing the velocity distribution (shaded for ebb tide) and the salinity distribution (shaded for salinity > 10 ppt) for June 9–10, 1991. The arrows labelled A indicate slack tide and the arrows labelled B indicate slack currents.

and 5% (Far Northern Channel) under strong trade winds (wind speed = 15 m^{-1}). This inequality is clearly not due to the Coriolis effects since in the southern hemisphere, Coriolis effects would deflect the plume away from the Southern Channel and toward the Far Northern Channel, *i.e.*, with the coast on the left of the plume. The uneven division of the freshwater discharge between the channels is responsible for the uneven salinity distribution in the three channels (Figures 1 and 11) resulting in the Southern Channel being less saline than the other two channels.

The 1 ppt isohaline is predicted be located 15 km farther landward in the Far Northern Channel under strong trade winds than in calm weather (Figure 11), and this prediction agrees well with observations (see the lines labelled Max and

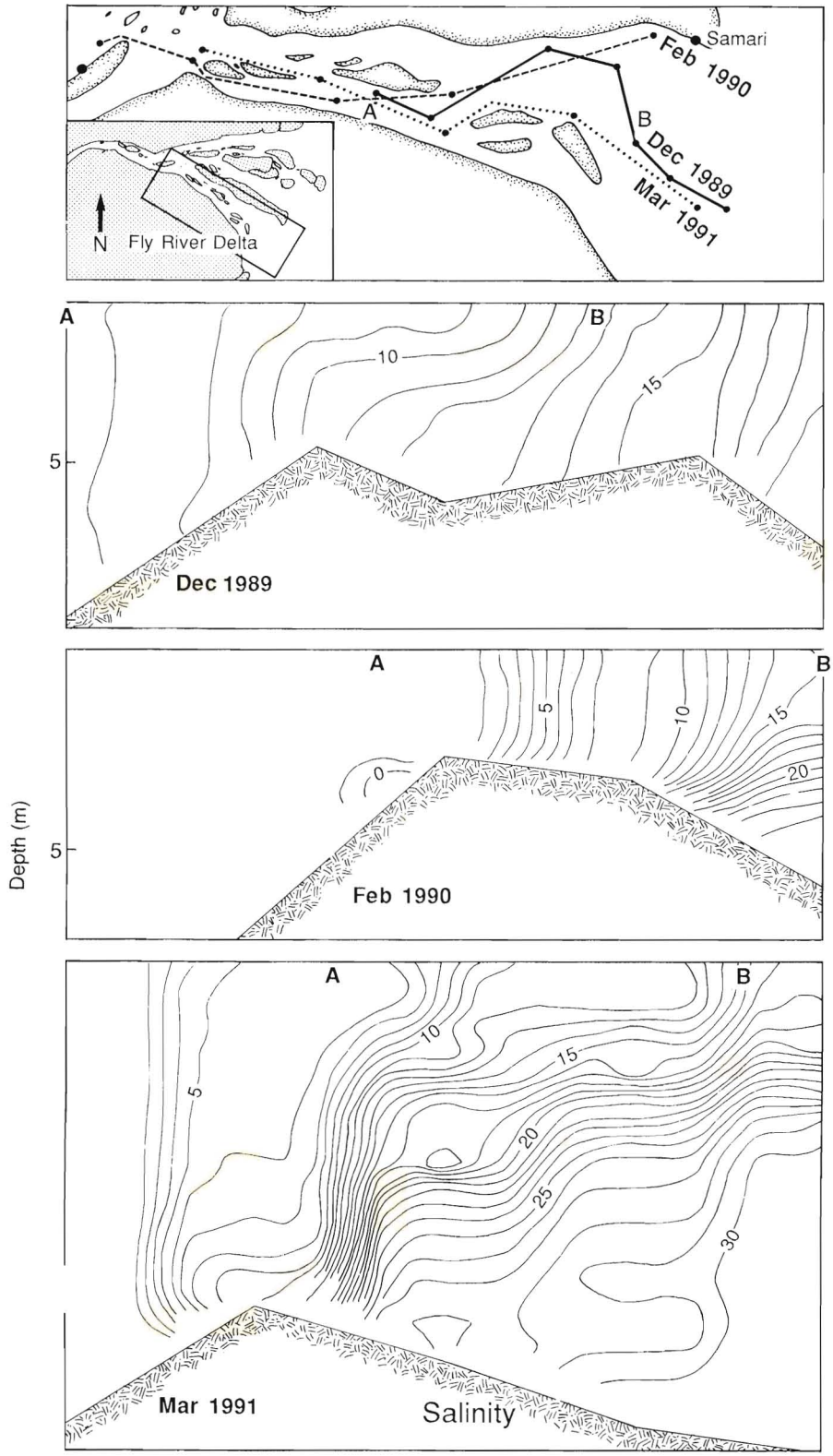

Figure 6. Location map of three along-channel transects in the Southern Channel with the measured distribution of salinity (ppt). Points A and B are reference locations to enable comparison between the graphs.

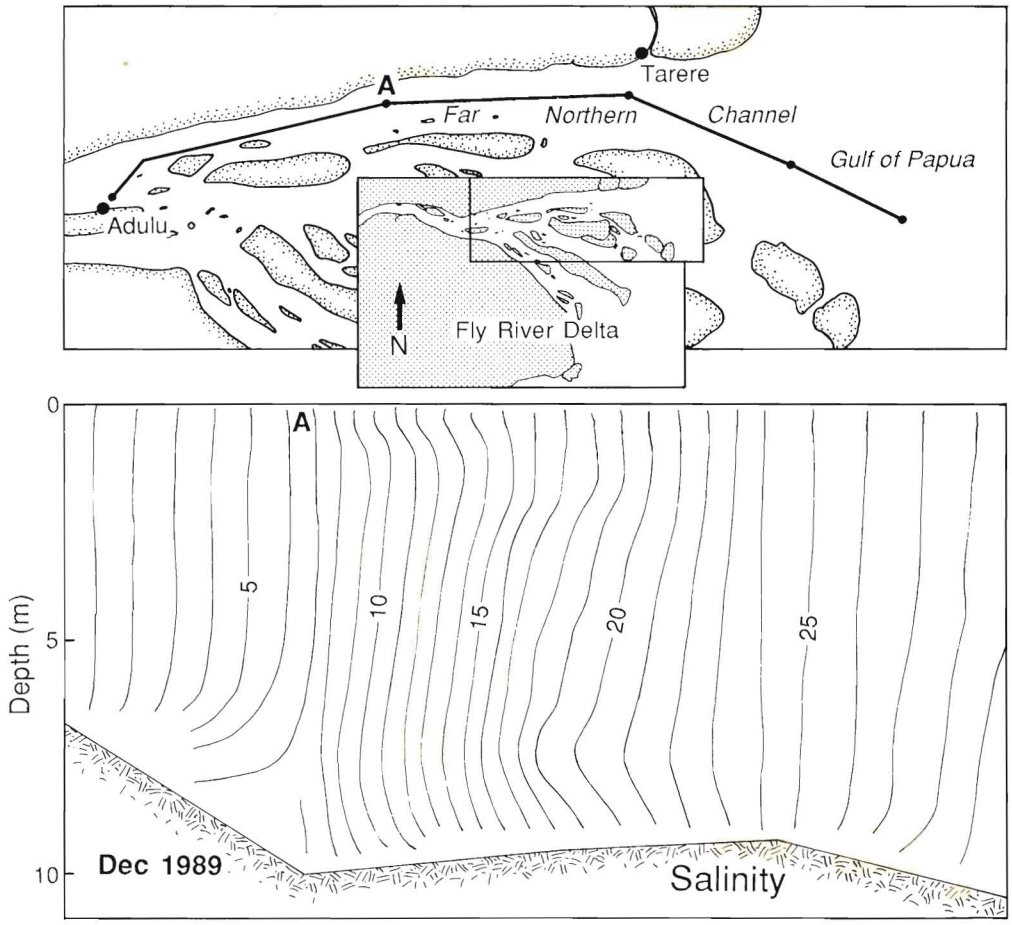

Figure 7. Location map of an along-channel transect in the Far Northern Channel and the corresponding distribution of salinity (ppt). Vertically well-mixed conditions prevailed in all our surveys of this channel.

Min lines in Figure 1). Under strong winds and spring tides, saline waters are predicted to intrude far enough around high spring tide into the Northern Channel for slightly saline water to intrude into the Southern Channel past the tip of Kiwai Island. This results in patches of low salinity (0.5–1 ppt) waters in the fresh water region of the Southern Channel (Figure 11). Such patches have been observed on occasions in the field.

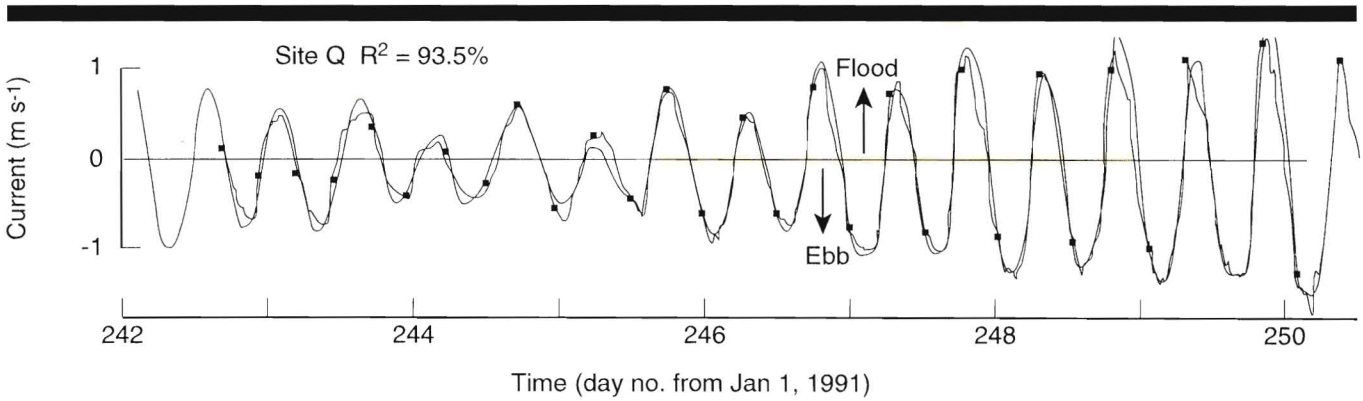

Figure 8. Time-series plot of the observed and predicted along-channel currents at site Q.

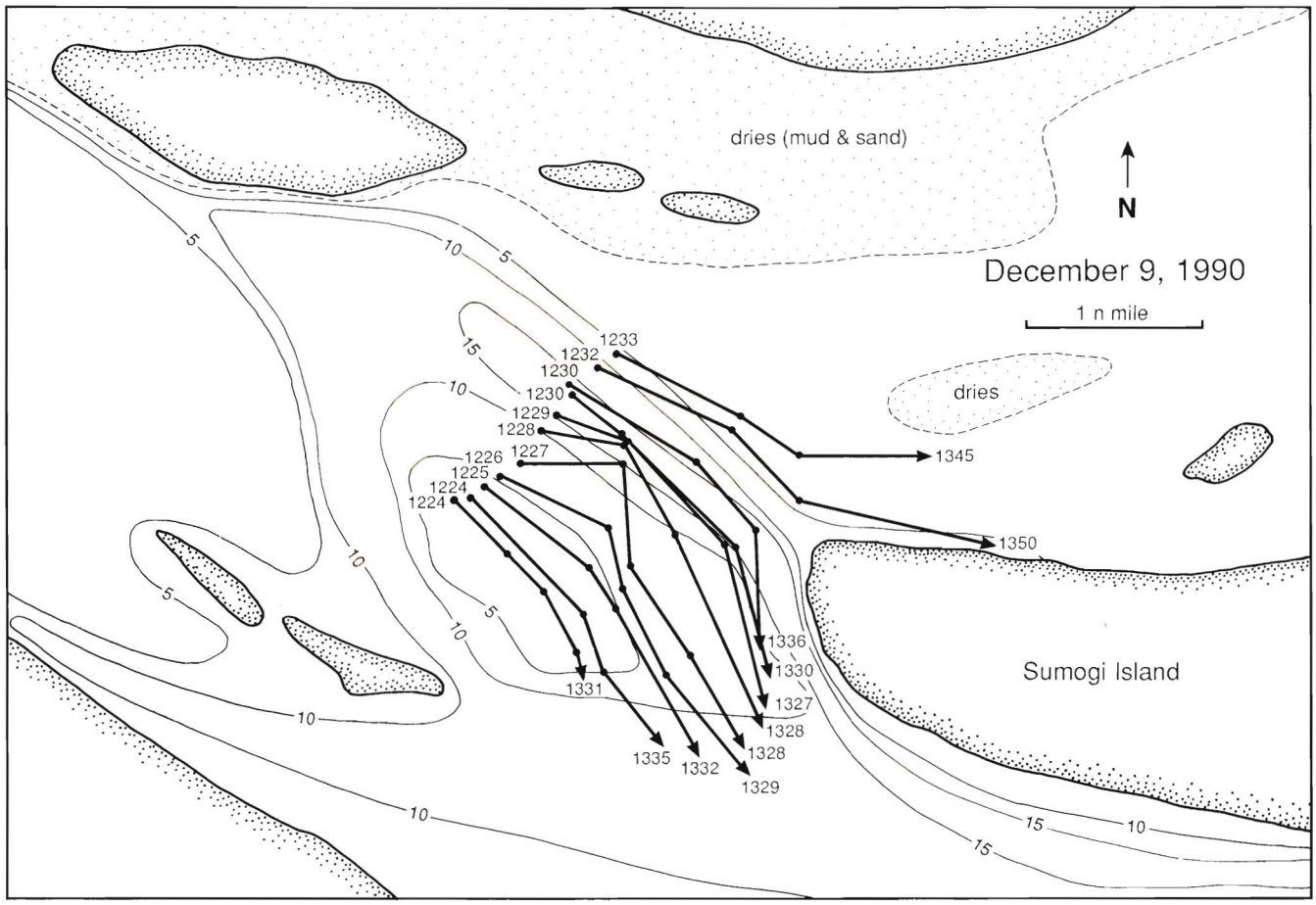

Figure 9. Bathymetry (depth in m) and plots of drogue trajectories. The 1 m × 2 m sail drogues were released at 2 m depth in freshwater and in calm weather at the ebb tide upstream of Sumogi Island which marks the division between the three major channels. The bulk of the flow was diverted south of Sumogi Island.

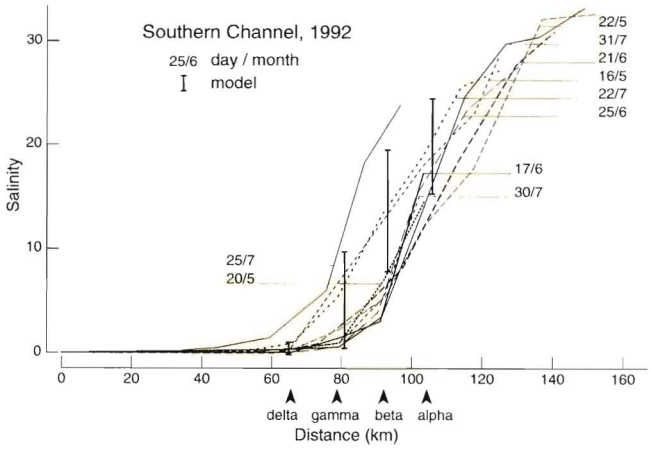

Figure 10. Along-channel distribution in the Southern Channel in 1992 of the salinity (ppt), both observed (depth-averaged) and predicted (the bars indicate the predicted fluctuations with the tides).

The model suggests that the dominant mechanism for salt intrusion is mixing by the lateral shear of the tidal currents (FISCHER *et al.*, 1979). The local horizontal diffusion coefficient, K_x, at the model's horizontal mesh size of 1200 m, turns out to be a key parameter. If K_x was set to unrealistically small values (maximum value < 0.2 m^2 s^{-1}), at flood tides intruding saline water propagated in the model preferentially in the deeper regions of the channels, saltier water remaining in the shallow waters over the shoals. A large cross-channel salinity gradient resulted, in conflict with observations. To reproduce the observations of negligible cross-channel salinity gradients, we had to take the minimum value of $K_x \geq 0.4$ m^{2}s^{-1} in the model, a value which is still realistic based on data from other estuaries (FISCHER *et al.*, 1979). With this value the predicted salinity shows minimal cross-channel variations (Figure 11). Higher values of K_x lead to higher values of the tidally-averaged along-channel diffusion coefficient and unrealistically high salinity intrusions.

The absence of strong cross-channel salinity gradients can thus be attributed to enhanced horizontal mixing due to the

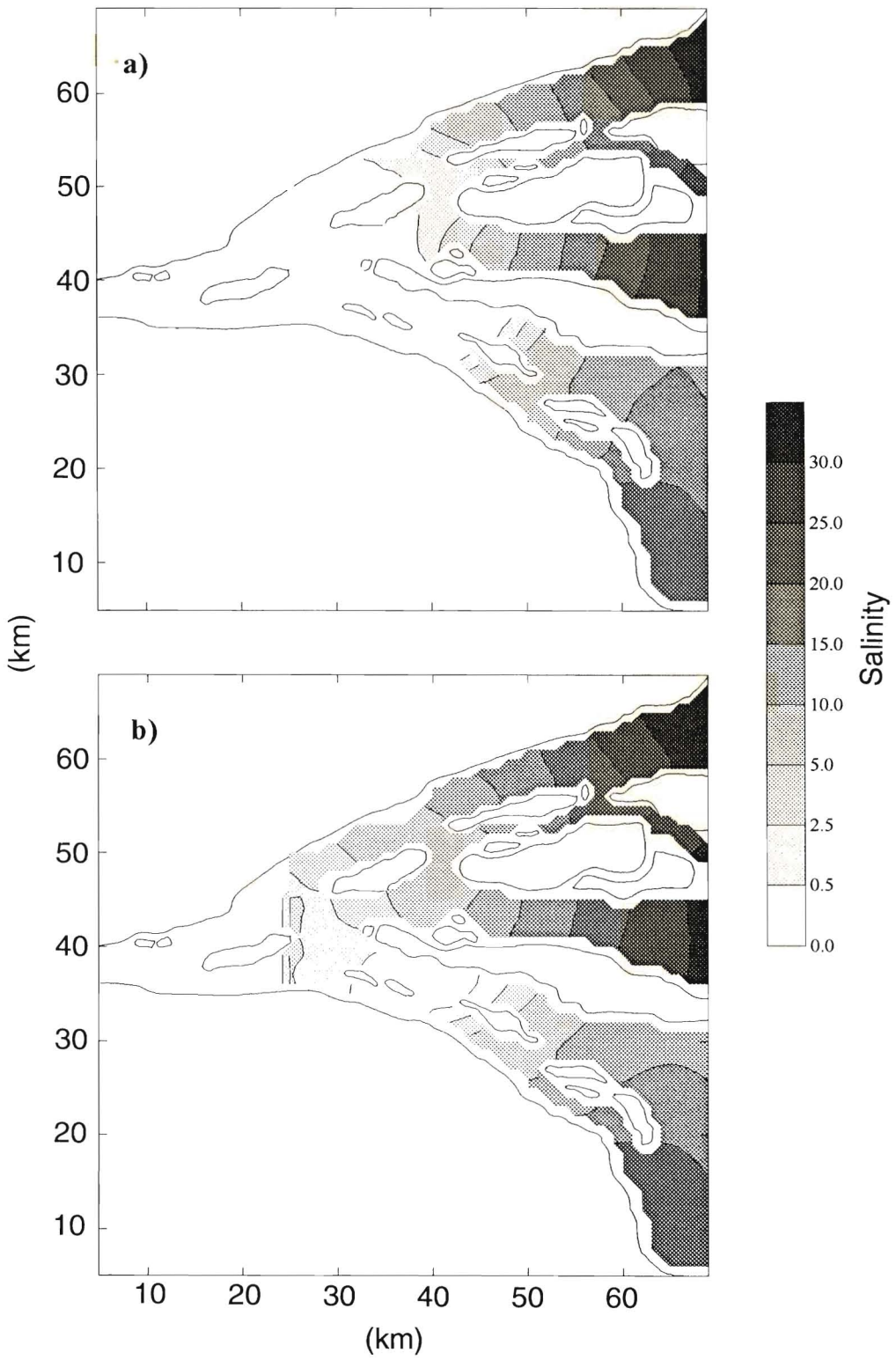

Figure 11. Synoptic distribution of the predicted salinity (ppt) at spring tides (a) in calm weather and (b) under 15 m s^{-1} southeast trade winds, for a freshwater discharge of 6,000 m^3s^{-1}.

lateral shear generated by the sinuosity of the thalweg meandering between numerous islands and shoals. By tracking freshwater particles in the model, the residence time of freshwater in the estuary was estimated to be about 3 weeks.

CONCLUSIONS

Field observations and numerical models were used to study the Fly River estuarine dynamics. The river discharge, the spring-neap tidal cycle, the wind and the presence of fluid mud are all important in determining the salinity distribution in the estuary.

Atmospheric and planetary tides forced by the Coral Sea are both important in determining the water level at the mouth. The atmospheric tides are typically 0. 1 m, are low-frequency (period > 5 days), and are experienced throughout the delta. The planetary tides at the river mouth are dominated by the diurnal and semi-diurnal tides.

At the apex of the delta, low-frequency water level fluctuations are larger than at the mouth because they also depend on the along-channel water level slope due to the freshwater discharge. As a result of this discharge, the low-frequency water level at the apex of the delta is typically 0.03 m higher than that at the mouth at neap tides. At spring tides and in calm weather this water level difference reaches 0.13 m. The reason for this spring-neap tide cycle in the low-frequency water level at the apex of the delta appears to be the spring-neap variation of the tidal current; this in turn generates a spring-neap fluctuation of the low-frequency bottom friction coefficient. Thus the water slope necessary to evacuate the freshwater input in the estuary varies with the tides, being largest at spring tides and smallest at neap tides. The trade winds blow parallel to the Far Northern Channel and add up to 0.1 m to the low-frequency water level at the apex of the delta, so that the difference in mean water level at the mouth and at the apex of the delta reaches 0.23 m. The difference between the low-frequency water level at the apex of the delta and at the mouth fluctuates in a predictable linear manner with the tides ($R^2 > 0.7$).

The currents are weaker in the Southern Channel than in the other channels, thus these other channels carry the bulk of the tidal energy. The tidal currents are successfully reproduced by a vertically-averaged, two-dimensional hydrodynamic model ($R^2 = 0.85 - 0.93$) provided that the Manning's friction coefficient, n, is assumed to be unusually small ($n = 0.015$, instead of 0.025 as is commonly used in sandy estuaries). This may be due to the presence of fluid mud in the estuary enabling the bulk of the water to slip over the fluidised bed.

The funnelling effect leads to an amplification of the tidal wave at the apex of the delta. Shallow water effects introduce a shoaling effect and generates important higher harmonics (e.g., the M_4 tide) for the tidal wave, giving rise to a pronounced tidal asymmetry.

Saline water intrudes the farthest in the Far Northern Channel, especially under strong trade winds when the saline intrusion limit moves a further 15–20 km upriver. The saltwater intrusion is much smaller in the Southern Channel and varies less with the wind. These observations were successfully reproduced by an advection-diffusion model, the advection being calculated by a depth-averaged hydrodynamics model and a simple laterally-averaged, quasi-steady, baroclinic model. Diffusion was modelled by a random walk model. The model suggests that the Southern Channel carries the bulk of the freshwater flux. This channel receives between 55% and 80% of the freshwater discharge, according to the wind. This asymmetry in turn controls the distribution of mangroves, mostly freshwater types in the Southern Channel and saltwater types in the Northern and Far Northern Channels.

The average residence time of freshwater in the estuary is predicted to be about 3 weeks.

The absence of strong cross-channel salinity gradients and of axial convergence zones is attributed to enhanced horizontal mixing by the lateral shear due to the sinuosity of the thalweg meandering around islands and shoals.

ACKNOWLEDGEMENTS

We thank Mr. M. Eagle, Dr. R. Higgins, Mr. I. Wood, Dr. R. Smith, Mr. K. Nabwakulea, Mr. J. Soles, Mr. M. Trenoden, Dr. P. Ridd, Mr. R. McAllister, and numerous other people including the ship crews, the helicopter pilots and the villagers who helped in supplying food and in deploying and recovering the tide gauges, they all made this study possible in a very difficult environment. This work was supported by Ok Tedi Mining Limited and the Australian Institute of Marine Science.

LITERATURE CITED

AUBREY, D.G., and FRIEDRICHS, C.T., 1988. Seasonal climatology of tidal non-linearities in a shallow estuary. Aubrey, D. and Weishar, L. (eds.): *Hydrodynamics and Sediment Dynamics of Tidal Inlets.* New York: Springer-Verlag, pp. 103–124.

FISCHER, H.B., LIST, E.J., KOH, R.C.Y., IMBERGER, J., and BROOKS, N.H., 1979. Mixing in inland and coastal waters. New York: Academic Press, 484p.

FISHER, J.S., DITMARS, J.D., and IPPEN, A.T., 1972. Mathematical simulation of tidal time-averages of salinity and velocity profiles in estuaries. *M.I.T. Sea Grant Project Report, MITSG72–11,* 193p.

FOREMAN, M.G.G., 1977. Manual for tide height analysis and prediction. *Pacific Marine Science Report 77–10.* Institute of Ocean Science, Patricia Bay, Sidney, British Columbia, 97p.

GODIN, G. 1972. *The Analysis of Tides.* Liverpool: Liverpool University Press, 264p.

OTML (OK TEDI MINING LIMITED), 1988. *Sixth Supplemental Agreement Environmental Study, 1986–1988.* Final Draft Report, Vols I, II & III (unpublished).

MOELLER, J.C. and ADAMS, E. 1993. Comparison of Eulerian and Eulerian-Lagrangian, random walk and hybrid methods of modeling pollutant transport. *Proceedings 3rd, International conference "Estuarine and Coastal Modeling III"* (American Society of Civil Engineers pp. 609–619.

PROVIS, D.G. and LENNON, G.W., 1983. Eddy viscosity and tidal cycles in a shallow sea. Estuarine, *Coastal and Shelf Science,* 31, 541–555.

RAUPACH, M. and MITCHELL, W. 1977. Time series analysis on the DEC-system 10. Flinders University of South Australia, *Flinders Institute for Atmospheric and Marine Science, Computing Report No. 10,* Adelaide, 87p.

SALOMONS, W. and EAGLE, A.M., 1990. Hydrology, sedimentology and the fate and distribution of copper in mine-related discharges in the Fly River system, Papua New Guinea. *The Science of the Total Environment,* 18, 291–314.

SMEC (SNOWY MOUNTAINS ENGINEERING CORPORATION), 1982. *Ok Tedi project. Hydrodynamic Survey of the Fly River.* Comma: Snowy Mountains Engineering Corporation report, 99p.

TAYLOR, L.W.H., 1973. A preliminary investigation of the marine geology of the Fly River estuary, Papua. Unpublished report, Department of Geology, University of Sydney, 18p.

TURRELL, W.B, and SIMPSON, J.H., 1988. The measurement and modelling of axial convergence in shallow well-mixed estuaries. in Dronkers, J. and Van Leussen, W. (eds.) *Physical Processes in Estuaries.* Berlin: Springer-Verlag, pp. 133–145.

WOLANSKI, E., 1994. Physical Oceanographic Processes of the Great Barrier Reef. Boca Raton, Florida: CRC Press, 194p.

WOLANSKI, E. and KING, B., 1990. Flushing of Bowden Reef lagoon, Great Barrier Reef. Estuarine, *Coastal and Shelf Science,* 31, 789–804.

WOLANSKI, E. and GIBBS, R.J., 1995. Flocculation of suspended sediment in the Fly River estuary, Papua New Guinea. *Journal Coastal Research,* 11, 754–762.

WOLANSKI, E. and EAGLE, M. 1991. Oceanography and fine sediment transport, Fly River Estuary and Gulf of Papua. *Proceedings 10th Australasian Conference on Coastal and Ocean Engineering,* (Auckland, New Zealand), pp. 453–457.

WOLANSKI, E., NORRO, A. and KING, B. 1994. Water circulation in the Gulf of Papua. *Continental Shelf Research,* 15, 185–212.

WOLANSKI, E., KING, B., and GALLOWAY, D. 1995. Dynamics of the turbidity maximum in the Fly River estuary, Papua New Guinea. *Estuarine, Coastal and Shelf Science,* 40, 321–337.